Journal of Marine Science and Technology

Volume 10 | Issue 2 Article 3

Monitoring of Sandstorms with ROCSAT-1 OCI Data

Shih-Jen Huang
Graduate Student (Huang and Kuo) Institute of Space Science, National Central University, Chung-Li, Taiwan 320.

Gin-Rong Liu
Professor (Liu) and Associate Research Engineer (Lin) Center for Space and Remote Sensing Research, National Central University, Chung-Li, Taiwan 320.

Tsung-Hua Kuo
Graduate Student (Huang and Kuo) Institute of Space Science, National Central University, Chung-Li, Taiwan 320.

Tang-Huang Lin
Professor (Liu) and Associate Research Engineer (Lin) Center for Space and Remote Sensing Research, National Central University, Chung-Li, Taiwan 320., thlin@csrsr.ncu.edu.tw

Chih-Kang Liang
Graduate Student (Liang) Institute of Atmospheric Science, National Central University, Chung-Li, Taiwan 320.

Monitoring of Sandstorms with ROCSAT-1 OCI Data

Acknowledgements

This research was supported by the National Science Council of Taiwan under grants NSC-88-NSPOA-OCI-019-01-02 and NSC-89-NSPO-A-OCI-019-01- 02. The authors also want to thank the Science Data Distribution Center of the Ocean Color Imager (OCISDDC) for their assistance in providing the OCI data used. In addition, we would like to extend out special thanks to Mr. Charlie Liang for his careful proofreading in improving the English writing.

MONITORING OF SANDSTORMS WITH ROCSAT-1 OCI DATA

Shih-Jen Huang*, Gin-Rong Liu**, Tsung-Hua Kuo*, Tang-Huang Lin**, and Chih-Kang Liang***

Key words: ocean color imager, sandstorm, aerosol optical depth.

ABSTRACT

The Ocean Color Imager (OCI) onboard the ROCSAT-1 Satellite was employed to demonstrate its capability in monitoring sandstorm events around Mongolia and northwestern China where they have been occurring in great frequency over these past few years. The OCI measures the radiance from the visible to near infrared regions in six spectral channels. The radiance can be used to calculate the aerosol optical depth (AOD) of the atmosphere through an atmospheric correction algorithm. The variation in the AOD during January and February of 2001 is investigated in this study. A set of OCI images covering the Yellow Sea was selected for analysis. The results showed that the AOD values increased significantly after the sandstorms erupted, where its value was almost four times higher than before.

INTRODUCTION

Simply put, the suspended particles in the air are called aerosols. They are produced either through natural processes or by human activities. Aerosols not only scatter, but also absorb significantly the incoming solar radiation within the entire spectrum [1]. They are also a provider of cloud condensation nuclei, which results in the formation of clouds and may thus affect the Earth's radiation budget. The amount of aerosol is closely related to the air quality. Due to the fact that these suspended particles affect the radiance transfer, the aerosol optical depth (AOD), a parameter in the radiation transfer equation, can be used to describe the optical properties of the aerosols.

Paper Submitted 08/06/01, Accepted 04/19/02. Author for Correspondence: Shih-Jen Huang.

**Graduate Student (Huang and Kuo) Institute of Space Science, National Central University, Chung-Li, Taiwan 320.*

***Professor (Liu) and Associate Research Engineer (Lin) Center for Space and Remote Sensing Research, National Central University, Chung-Li, Taiwan 320. E-mail: thlin@csrsr.ncu.edu.tw*

****Graduate Student (Liang) Institute of Atmospheric Science, National Central University, Chung-Li, Taiwan 320.*

Since the 1960s, satellite-borne sensors in the visible and infrared (IR) regions have been considered an innovative tool in investigating the atmospheric air quality. Durkee *et. al*. [2] derived the AOD and aerosol size distribution for global analysis by using the Advance Very High Resolution Radiometer (AVHRR) data with band ratios of the red and near-infrared channels. Holben *et. al*. [3] selected the dark areas of AVHRR data to retrieve land aerosols. Liu *et. al*. [4] used SPOT data to retrieve the aerosol characteristic parameters and surface reflectance. The measurement of the AOD over the ocean with AVHRR data [5,6] has even become a routinely operation for the National Oceanic and Atmospheric Administration (NOAA). In recent years, the satellite observation data quality has risen to a level where the monitoring of the air quality, ecology, and environment is considered acceptable [7].

In addition to the NOAA and SPOT satellite data, the space borne ocean color sensors (e.g., CZCS, SeaWiFS) are also used in monitoring our environment. Fukushima and Toratani [8] developed a semi-empirical optical model to estimate the aerosol single-scattering albedo and to improve the atmospheric correction algorithm by using the Coastal Zone Color Scanner (CZCS,1978-1986). Wang *et. al*. [9] used the Sea-viewing Wide Field-of-view Sensor (SeaWiFS) data to retrieve monthly composite images of the global aerosol optical property with spectral channels from 765nm to 865nm. Since OCI is a SeaWiFS-like sensor, it too has the capability in monitoring the air quality [10].

The OCI sensor is placed onboard the ROCSAT-1 satellite, which was launched into a low-earth orbit in January 1999. It has an altitude of 600km with an inclination angle of 35°, and owns an orbital period of 97 minutes. It beams downlink telemetry signals to the surface receiving station six times a day. The OCI sensor provides six channels at 443nm, 490nm, 512nm, 555nm, 670nm and 865nm where an additional channel centered at 555nm is used to evaluate the condition of radiometric decay with time for the former six channels. The OCI is a push-broom scanner owning a 700-kilome-

ter field-of-view with 896 pixels in each line. The spatial resolution is 400 meters for the 64 pixels located at the center, and 800 meters for the remaining ones (Table 1).

ROCSAT-1 was designed mainly to carry out the scientific experiments related to the oceanic and atmospheric environments, which include three main categories—ocean color imaging, studying the ionospheric plasma and its electrodynamics, and communications in the Ka-band. The primary mission of the OCI sensor is providing observational data for the analyses of the marine and atmospheric environment [11].

Sandstorms occur over Mongolia and the arid regions of northwestern China virtually each year. [12]. From January to February 2001 alone, three major sandstorms were recorded over northwestern China [13]. Past records revealed that these events occurred unusually earlier, and were more frequent and powerful than before. The sandstorms were induced by the strong south-moving Siberian cold air mass, which significantly degenerated the air quality over the western Pacific region including China, Korea, Japan and Taiwan. The phenomenon even affected the air quality over portions of North America [14]. Therefore, it may be inferred that the occurrence of the sandstorms around the arid areas of northwestern China can affect regions in a global scale. Finding ways to monitor and evaluate their influences on the Pacific region, especially through satellite-borne observations, is becoming an increasingly important topic. In this paper, the ROCSAT-1/OCI images will be used to estimate the AOD and delineate the time variation of the AOD over the Yellow Sea.

Table 1. The parameters of ROCSAT-1/OCI

Parameters	Description
Inclination	35°
Altitude(km)	600
Period(min)	96.7
Spectral bands(nm)	B1 443-453
	B2 480-500
	B3 500-520
	B4 545-565
	B5 660-680
	B6 845-885
Ground resolution(m^2)	800×800
Swath width(km)	702
Total pixels per scan line	896
Observation method	Push broom
Acquisition time (local)	9:00-15:00
Tilt	no
Launch date	Jan. 1999

DATA AND METHODOLOGY

The occurrence of a sandstorm can be observed by estimating the atmosphere's AOD. Hence, calculations of the AOD were conducted by monitoring the radiometry of the atmosphere from images acquired by OCI. In order to quantitatively compare the variations before and after the sandstorm event, effects of the Mie (suspended particle) scattering and Rayleigh (atmosphere molecules) scattering are separated from the total radiance observed by OCI.

In this study, the single scattering approximation was employed [15] under the consideration of simplifying the mathematical modeling and reducing the calculation time. The aerosol radiance in the single scattering mode observed by OCI at the top of the atmosphere in the visible and NIR regions can be simplified by

$$L_a(\lambda) = \frac{\omega_a(\lambda)\tau_a(\lambda)F_0^{'}(\lambda)P_a}{4\pi\cos\theta} \tag{1}$$

where ω_a is the aerosol single scattering albedo, λ is the wavelength, τ_a is the aerosol optical depth, P_a is a parameter which is dependent on the scattering phase function and Fresnel reflectance, θ is the zenith angle. $F_0^{'}$ is the instantaneous extraterrestrial solar irradiance after it is weakened by the atmosphere, such as

$$F_0^{'}(\lambda) = F_0(\lambda)T(\lambda)$$

$$F_0(\lambda) = \overline{F}_0(\lambda)\left[1 + 0.0167\cos\frac{2\pi(D-3)}{365}\right] \tag{2}$$

where T is the total transmittance, $\overline{F}_0$ is the extraterrestrial average solar irradiance, and D represents Julian days. In our computation, the Henyey-Greenstein aerosol scattering phase function [16] was used for marine aerosol type. The multiple aerosol scattering mode was further assessed by using a linear transformation [17], the radiance L was changed to the reflectance ρ_{sa} such as

$$\rho_{sa}(\lambda) = \frac{\pi L_a(\lambda)}{F_0\cos\theta_0} \tag{3}$$

$$\rho_{ma}(\lambda) = I(\lambda) + S(\lambda)\rho_{sa}(\lambda) \tag{4}$$

where ρ_{sa} is the reflectance of the single aerosol scattering, ρ_{ma} is the reflectance of multiple aerosol scattering, F_0 is the extraterrestrial solar irradiance, and θ_0 is the solar zenith angle. $I(\lambda)$ and $S(\lambda)$ are the intercept and the slope, respectively. The parameters were each obtained from the LOWTRAN-7 model [18].

The Angstrom formulation for the aerosol optical depth is

$$\tau_a(\lambda) = \beta\lambda^{-\alpha} \tag{5}$$

where α is the Angstrom exponent, and is related to the Junge exponent. The Junge exponent describes the slope of the aerosol size distribution, while β is the turbidity coefficient, representing the aerosol concentration.

The aerosol albedo of the single scattering, $\omega_a(\lambda)$, was estimated [19, 20] by,

$$\omega_a(0.55) = (-0.0032AM + 0.972)\exp(3.06 \times 10^{-4}RH) \quad (6)$$

$$\omega_a(\lambda) = \omega_a(0.55)\exp[-0.095[\ln(\lambda/0.4)]^2 + 0.0096342] \quad (7)$$

where *RH* is the relative humidity of the atmosphere obtained from the Comprehensive Ocean-Atmosphere Data Set (COADS) of the National Center for Atmospheric Research (NCAR). *AM* is the air mass character. Generally speaking, *AM* can be used as an indicator for quantifying the aerosol type over the ocean producing a scale from 1 to 10, where 1 stands for the open ocean (clear air quality), and 10 for coastal areas (rather poor air quality). The *AM* character is strongly influenced by natural or industrial aerosols originating from neighboring continents [21].

In determining the *AM* values during the time of acquisition, this study employed the Lowtran-7 model to simulate the total radiance observation by the six channels of OCI under different observation and atmospheric conditions. The observation geometry and time of observation, sea surface albedo, and different air mass characters, were compiled into a database. The channels at 670nm and 865nm were then used to aid the assessment of the aerosol scattering effect and the air mass character parameter in the Lowtran model. The total radiance observed by the ROCSAT sensor was then compared with the database. The sea surface albedo and AM values that matched with the database were chosen as the observation conditions during the satellite flyby (Fig. 1). After the parameters were determined, the AOD of the aerosols could be computed.

RESULTS

Generally, the Asian sandstorms that originated from northwestern China and Mongolia moved southeastwardly with the winter-spring circulations, which significantly deteriorated the air quality over the Eastern Asian area. Parts of North America were also affected where some of the particles were carried along in the easterly stream. In this study, a 1° latitude × 1° longitude area near the Yellow Sea centered at 35.5° N, 122.0° E was selected as the observation area (Fig. 2) to investigate the effects on the AOD values.

Due to the limited operational time and rather unique special orbit, OCI is unable to maintain a high revisit rate. In addition, sun-glint and cloudy pixels must be excluded in advance. Therefore, gathering a set of high temporal resolution images of the OCI was not easy. Eventually, a collection of nine qualified OCI images was selected and processed by our atmospheric correction and AOD retrieval algorithm. Before processing, we also performed a cloud-masking procedure for any cloud-contaminated pixels.

As discussed previously, the satellite observed radiance is contributed both by scattering from atmospheric molecules or aerosols and reflectance from the earth's surface. The radiance component of the atmospheric molecules should be removed from the observed radiance in order to reveal the actual radiance component contributed by the sandstorm particles. After the Rayleigh scattering was eliminated, the sandstorm effect could be qualitatively demonstrated (Fig. 2). The pseudo-color images were composed by the OCI chan-

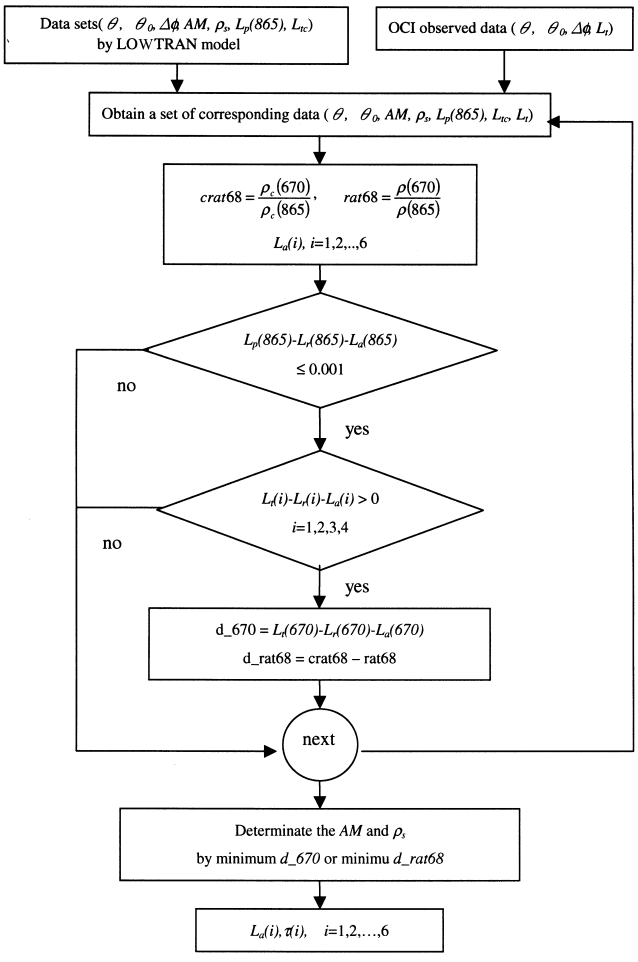

Fig. 1. The flow chart of air mass character (*AM*) and sea surface albedo (ρ_s) determination.

nels at 443nm (B), 555nm(G) and 670nm(R). For better visualization, the cloudy pixels were not masked in the pair. The images cover the Shan-Tung Peninsula of eastern Mainland China and the East China Sea. Fig. 2 (a) shows a clear image acquired before a major sandstorm was recorded on January 31, 2001. Both the textures of the land topography and the borders of the land/sea border can be clearly identified. Meanwhile, the image also shows a darker tone, revealing that the air was clearer because the scattering effect was small over the land and sea area. Contrary to the former image, Fig 2(b) acquired two days later after the sandstorm event, indicates a brighter tone in the image, revealing a much stronger scattering effect in the aerosol component. From these Rayleigh corrected images; the effects of the particles from the sandstorms on the atmosphere can be clearly demonstrated. Meanwhile, we further investigated spatial variation of the radiance along a latitudinal line. In this study, a strip along the 37° N latitude was analyzed. In order to illustrate clearly the radiance variance with the longitude, the mean radiance was obtained from a succession of $0.1° \times 0.1°$ windows along the 37° N latitude between longitude 110° E to 135° E. Fig. 3 shows the result from the 555nm channel. Each dot in the figure represents the mean radiance of a $0.1° \times 0.1°$ area. As mentioned earlier, the radiance rose significantly after the sandstorm event, either over the land or sea area where clouds were not detected. Although the cloudy pixels were not excluded in this step, the radiance variation could still be seen. The comparison shows that the Mie scattering radiance greatly increased after the sandstorm event. Detailed comparison with cloud free pixels revealed that the sea had a low radiance count, because the land surface reflectance was greater than that on the sea surface, around 110° E to 122.4° E (Mainland China) and 126.3° E to 129.4° E (Korea). By comparing the radiance before and after the sandstorm event, it could be more clearly distinguished from the ocean area.

Finally, we analyzed the temporal variations of the effects produced by the sandstorm particles of the observational area, as shown in Fig. 2. The AOD values retrieved from the OCI observation from the end of January to the middle of February of 2001 are shown in Fig. 4. In this figure, all cloud-contaminated pixels were masked before comparing the actual AOD values contributed by aerosol particles. The results show a drastic increase in the AOD after January 30, 2001 because a sandstorm occurred in Mongolia on January 31, 2001. The AOD value attained its highest level on February 4 and dropped very slowly afterwards. During our study period, no major forest fire or volcanic eruptions was reported. This reveals clearly that the sand-

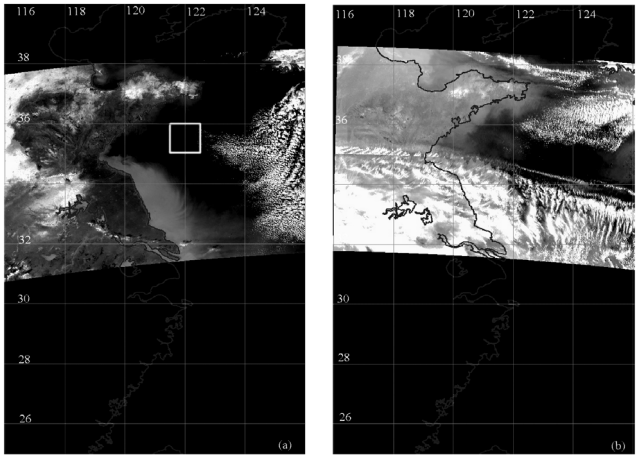

Fig. 2. The comparison of OCI pseudo-color images acquired on (a) 2001/01/29 07:26Z (before sandstorm), and (b) 2001/02/02 06:49Z. The white square area is the observational area of this study, where its center location is (35.5°N, 122.0°E).

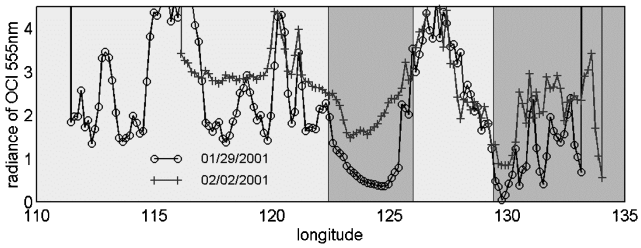

Fig. 3. The comparison of the radiance observed by the OCI excluding the Rayleigh scattering component before (circle line)/after (plus line) at 555 nm along the 37°N latitude. The bright background expresses the land area, while the dark background represents the sea area.

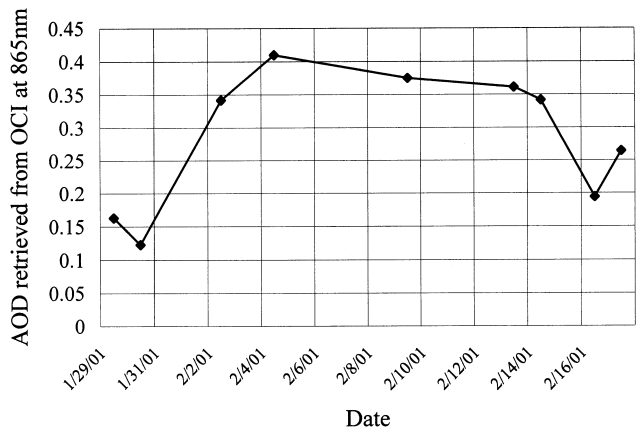

Fig. 4. The variation of the mean AOD over the observational area. Some dates are empty either because the satellite did not perform a flyover or clouds were detected.

storm particles were the main contributor to the AOD changes. In the result, the AOD value rose almost four times higher (from 0.12 up to 0.41). The high AOD indicated high aerosol particle concentration, which were comprised mostly of sand or dust that were thrown into the sky by the strong turbulent winds in Mongolia and then carried out by the Asia winter monsoon.

CONCLUSIONS

In this study we have proposed a scheme for monitoring Asian sandstorms with the ROCSAT-1/OCI data. The air quality can be distinguished from the pseudo-color OCI images in eastern Asia. The pseudo-color images show a deeper tone under clear sky conditions and brighter tones after the eruption of the sandstorm. The stronger scattering effect is caused by the suspended particles from the sandstorm. It may also be inferred that the sandstorm is easier to be distinguished over the ocean when the Raleigh effect is excluded, because the ocean surface is more uniform and owns a lower reflectance than over the land.

The AOD values at the Yellow Sea produced a range from 0.12 to 0.41 during our study period. They rose almost four times higher while the sandstorm occurred. The high AOD values exhibit the high aerosol particles concentration suspended in the air. Therefore, the OCI data can be used to delineate the region under influence and also measure the extent of the Asian sandstorm. The developed AOD algorithm in this study can only be applied over a cloud free ocean. A suitable algorithm to retrieve the AOD over the land will be developed in the near feature.

ACKNOWLEDGEMENTS

This research was supported by the National Science Council of Taiwan under grants NSC-88-NSPO-A-OCI-019-01-02 and NSC-89-NSPO-A-OCI-019-01-02. The authors also want to thank the Science Data Distribution Center of the Ocean Color Imager (OCI-SDDC) for their assistance in providing the OCI data used. In addition, we would like to extend out special thanks to Mr. Charlie Liang for his careful proofreading in improving the English writing.

REFERENCES

1. Liou, K. N., "*An introduction to atmospheric radiation*", Academic Press, New York, pp. 234-292 (1980).
2. Durkee, P.A., F. Pfeil, E. Frost, and R. Shema, "Global analysis of aerosol particle characteristics", *Atmos. Environ.*, Vol. 25A, pp. 2457-2471 (1991).
3. Holben, B. N., E. Vermote, Y. J. Kaufman, D. Tanre, and V. Kalb, "Aerosol retrieval over land from AVHRR data application for atmospheric correction," *IEEE Transactions on Geoscience and Remote Sensing*, Vol. 30, No. 2, pp. 212-222 (1992).
4. Liu, C.H., A. J. Chen, and G. R. Liu, "An image-based retrieval algorithm of aerosol characteristics and surface reflectance for satellite images", *Int. J. Remote Sens.*, Vol. 17, No. 3477-3500 (1996).
5. Rao, C.R.N., L.L. Stowe, and E.P. McClain, "Remote sensing of aerosols over the oceans using AVHRR data Theory, practice and applications". *Int. J. Remote Sensing*, Vol. 10, No. 4, pp. 743-749 (1989).
6. Ignatov, A. M., L.L. Stowe, S. M. Sakerin, and G.K. Korotaev, "Validation of the NOAA/NESDIS satellite aerosol product over the North Atlantic in 1989". *J. Geophy. Res.* Vol. 100, No. D3, pp. 5123-5132 (1995).
7. King, D. M., Y. J. Kaufman, D., Tanre, and T. Nakajima, "Remote Sensing of Tropospheric Aerosols from Space: Past, Present, and Future," *Bull. Amer. Meteorol. Soc.*, Vol. 80, pp. 2229-2259 (1999).
8. Fukushima, H. and M. Toratani, "Asian dust aerosol: optical effect on satellite ocean color signal and a scheme of its correction", *J. Geophy. Res.*, Vol. 102, No. D14, pp. 17119-17130 (1997).
9. Wang, M.H., S. Bailey, and C. R. McClain, "SeaWiFS provides unique global aerosol optical property data". *EOS, Trans. AGU*, 81, pp. 197-202 (2000).
10. Huang, S.J. and G.R. Liu, "Derivation of aerosol optical thickness over the East Asian oceans with ROCSAT-1 OCI imagery", *ACRS2000 proceedings of the 21th Asian conference on remote sensing*, Taipei ROC, 2,777-781 (2000).
11. Yang, B. T., "The first ocean remote sensing payload of the ROC: an introduction", in *COSPAR Colloquium, Space Remote Sensing of Subtropical Oceans*, Taipei, Taiwan, 13A2-1-13A2-9 (1995).
12. Qiu, J. and L. Yang, "Variation characteristics of atmospheric aerosol optical depths and visibility in North China during 1980-1994," *Atmos. Environ.*, Vol. 34, pp. 603-609(2000).
13. Xinhua New Agency, "http://www.enviroinfo.org.cn" News release of 2001/01/31 and 2001/02/01, China (2001).
14. Visible Earth Browser in NASA, "http://visibleearth. nasa.gov/cgi-bin/ viewrecord?7936" (2001).
15. Buglia, J. J., "*Introduction to the Theory of Atmospheric Radiative Transfer*," Chapter 5, NASA reference publication 1156, 59-103 (1986).
16. Gordon, H. R. and D. J. Castano, "Coastal Zone Color Scanner atmospheric correction algorithm: multiple scattering effects," *Appl. Opt.*, Vol. 26, No. 2111-2122 (1987).
17. Gordon, H.R. and M. Wang, "Retrieval of water-leaving radiance and aerosol optical thickness over the oceans

with SeaWiFS: a preliminary algorithm", *Appl. Opt.*, Vol. 33, pp. 443-452(1994).
18. Kneizys, F. X., E.P. Shettle, L.W. Abreu, G.P. Anderson, J.H. Chetwynd, W.O. Gallery, J.E.A. Selby, and S.A. Clough, "User guide to LOWTRAN 7", *AFGL-TR 880177 Environmental Research Papers*, No. 1010 (1988).
19. Gregg, W. W. and K. L. Carder, "A simple spectral solar irradiance model for cloudless maritime atmospheres", *Limnology and Oceanography*, Vol. 35, No. 8, pp. 1657-1675 (1990).
20. Bird, R. E., and C. Riordan, " Simple solar spectral model for direct and diffuse irradiance on horizontal and tilted planes at the earth's surface for cloudless atmospheres", *J. Climatol. Appl. Meteorol*. Vol. 25, pp. 87-97 (1986).
21. Gathman, S.G. "Optical properties of the marine aerosol as predicted by the Navy model", *Optical Engineering* Vol. 22, pp. 57-62 (1983).